1   **One dose of COVID-19 nanoparticle vaccine REVC-128 provides protection against SARS-**

2   **CoV-2 challenge at two weeks post immunization**

3   Maggie Gu[1], Jonathan L. Torres[2], Jack Greenhouse[3], Shannon Wallace[4], Chi-I Chiang[5],

4   Abigail M. Jackson[2], Maciel Porto[3], Swagata Kar[3], Yuxing Li[5,6], Andrew B. Ward[2] and

5   Yimeng Wang[1,5,7*]

6   [1]ReVacc Scientific, Frederick, MD

7   [2]Department of Integrative Structural and Computational Biology, The Scripps Research

8   Institute, La Jolla, CA

9   [3]Bioqual, Rockville, MD

10   [4]Experimental Pathology Laboratories, Sterling, VA

11   [5]Institute for Bioscience and Biotechnology Research, Rockville, MD

12   [6]Department of Microbiology and Immunology and Center of Biomolecular Therapeutics,

13   University of Maryland School of Medicine, Baltimore, MD

14   [7]ReVacc Biotech, Frederick, MD

15   *Corresponding author: Yimeng Wang, ReVacc Biotech, 4539 Metropolitan Court, Frederick,

16   MD 21704, USA.

17   E-mail: yimengwang@revaccbio.com (YW)

18   Phone: +1 240-888-9816, FAX: +1 301-694-2999

19 **Abstract**

20   A COVID-19 vaccine with capability to induce early protection is needed to efficiently

21 eliminate viral spread. Here, we demonstrate the development of a nanoparticle vaccine candidate,

22 REVC-128, in which multiple trimeric spike ectodomain subunits with glycine (G) at position 614

23 were multimerized onto a nanoparticle. In-vitro characterization of this vaccine confirms its

24 structural and antigenic integrity. In-vivo immunogenicity evaluation in mice indicates that a

25 single dose of this vaccine induces potent serum neutralizing antibody titer at two weeks post

26 immunization, which is significantly higher than titer induced by trimeric spike protein without

27 nanoparticle presentation. The comparison of serum binding to spike subunits between animals

28 immunized by spike with and without nanoparticle presentation indicates that nanoparticle prefers

29 the display of spike RBD (Receptor-Binding Domain) over S2 subunit, likely resulting in a more

30 neutralizing but less cross-reactive antibody response. Moreover, a Syrian golden hamster in-vivo

31 model for SARS-CoV-2 virus challenge was implemented at two weeks post a single dose of

32 REVC-128 immunization. The results show that vaccination protects hamsters against SARS-

33 CoV-2 virus challenge with evidence of steady body weight, suppressed viral loads and alleviation

34 of tissue damage (lung and nares) for protected animals, compared with ~10% weight loss, higher

35 viral loads and tissue damage in unprotected animals. Furthermore, the data show that vaccine

36 REVC-128 is thermostable at up to 37°C for at least 4 weeks. These findings, along with a long

37 history of safety for protein vaccines, suggest that the REVC-128 is a safe, stable and efficacious

38 single-shot vaccine candidate to induce the earliest protection against SARS-CoV-2 infection.

39   SARS-CoV-2, the virus causing the COVID-19 pandemic, is a new emerging virus. SARS-

40   CoV-2 belongs to the coronavirus family with members including severe acute respiratory

41   syndrome coronavirus (SARS, 2003 strain), Middle East respiratory syndrome (MERS) and others

42   causing the common cold. The development of vaccine candidates focuses on the spike (S) protein

43   of the SARS-CoV-2 virus, which forms homotrimers protruding from the virus surface and

44   mediates virus entry by targeting angiotensin receptor 2 (ACE2) as the receptor[1] and heparin as

45   co-receptor. S protein is comprised of two functional subunits: S1 for receptor binding and S2 for

46   mediating fusion of the viral and cellular membranes (Fig. 1A). For SARS-CoV-2, S protein is

47   cleaved at the boundary (S1/S2) between S1 and S2, which remains non-covalently bound in the

48   prefusion conformation[2] (Fig. 1B). The S1 subunit comprises the N-terminal domain (NTD) and

49   receptor binding domain (RBD), while S2 subunit contains the fusion machinery with fusion

50   peptide (FP) located downstream of the cleavage site (Fig. 1A). The second cleavage at the S2'

51   site within the S2 subunit leads to a conformational change to initiate the membrane fusion[3] (Fig.

52   1A). The discovery of neutralizing monoclonal antibodies (nAbs) reveals a number of vulnerable

53   sites of the virus. Currently, most of the discovered nAbs have been reported to target the RBD[4-8]

54   and NTD[4,9], in contrast to a small number of nAbs targeting the S2 subunit[9]. In particular, the

55   footprint of the most potent nAbs usually lines within the epitope for ACE2 binding on the RBD,

56   suggesting that RBD is a desirable neutralizing epitope on virus spike protein.

57   Vaccines with a multivalent display of antigen are believed to induce longer-lasting

58   immunity than monovalent antigens[10,11]. Multivalent display using virus-like particle (VLP) or

59   nanoparticle (NP) is the common strategy for vaccine development, such as the VLP comprising

60   an array of 360 copies of the L1 capsid protein for the licensed HPV vaccine[12], or the eOD-GT8

61   60mer HIV-1 vaccine currently in clinical trials[13,14]. Spike protein or RBD of SARS-CoV-2

62   conjugated on NP were shown to elicit potent neutralizing antibody responses[15,16]. The Novavax

63   COVID-19 nanoparticle vaccine, NVX-CoV2373, induced protection for mice[17] and macaques[18]

64   against viral challenge and showed 89.3% efficacy in a Phase 3 clinical trial conducted in the UK,

65   by using a two-dose regimen. *Helicobacter pylori* ferritin has been used to display antigens from

66   influenza[19,20], hepatitis C virus[21], HIV-1[22,23], Epstein-Barr virus[24] and SARS-CoV-2[25]. Ferritin is

67   a highly conserved protein with a 24-subunit protein shell. Very recently, Powell et al.[25] reported

68   that ferritin display of SARS-CoV-2 spike ectodomain is able to induce a potent neutralizing

69   antibody response in mice. Similarly, influenza ferritin vaccines have been shown to be safe in

70   clinical trials (NCT03186781 and NCT03814720).

71   In this study, we developed a COVID-19 nanoparticle vaccine, designated as REVC-128

72   (or spike NP) with trimeric spike ectodomain subunits (glycine substitution at residue 614)

73   multimerized onto the ferritin nanoparticle. The design of this vaccine is aimed to preferentially

74   present the neutralizing antibody epitope (RBD) but occlude the S2 subunit to the immune system.

75   Such design elicits the neutralizing antibody response over cross-reactive antibody, which might

76   minimize antibody-dependent enhancement (ADE) concern (see Discussion section). We

77   compared the immunogenicity of spike NP versus spike non-NP (soluble trimeric spike protein

78   without nanoparticle presentation) and observed that a single dose of spike NP induced

79   significantly higher neutralizing but less S2 subunit-specific or cross-reactive antibody titers than

80   spike non-NP in mice. Encouraged by the observation of a high neutralizing antibody titer (10^4

81   ID_{50} of serum dilution) induced by spike NP at two weeks post immunization, we sought to

82   evaluate the protection efficacy of one-dose regimen with virus challenge. The in-vivo protection

83   efficacy study in hamsters showed that vaccinated animals slightly gained body weight from 4

84   days post infection, while the sham group lost ~10% weight by 7 days post infection. To our

85   knowledge, REVC-128 is the first COVID-19 vaccine to show evidence of vaccine induced-

86   protection starting at two weeks post immunization in this virus challenge model, which is earlier

87   than other vaccine candidates showing induced-protection starting at or after four weeks post first

88   dose of immunization (see Discussion section).

89

90   **Results**

91   **Generation of trimeric spike protein with or without nanoparticle presentation.** We first

92   expressed SARS-CoV-2 spike ectodomain residues 1 to 1208 in trimeric form by appending a T4

93   fibritin trimerization motif to the c-terminus of spike ectodomain. The ectodomain contains a

94   glycine substitution at residue 614 to match viral predominant isolate circulating in the middle of

95   2020[26-28], a "SGAG" substitution at the furin cleavage site (residues 682-685) to knockout furin

96   cleavage, and two proline substitutions at residues 986 and 987 to increase stability[29] (Fig. 1A).

97   The trimeric ectodomain protein was further multimerized onto ferritin with a linker to generate a

98   nanoparticle (NP) presenting trimeric spike protein. Trimeric spike proteins with or without NP

99   presentation were referred to spike NP (also designated as REVC-128) or spike non-NP,

100   respectively in the following. We first characterized spike NP or spike non-NP on size-exclusion

101   chromatography (SEC) with overlapping profiles showing that spike NP (red) was significantly

102   larger than spike non-NP (blue) (Fig. 1C). Spike NP displayed a clear sharp peak, while spike non-

103   NP displayed two peaks that we assigned to a minor aggregates peak and a predominant trimer

104   fraction peak (Fig. 1C). Negative stain electron microscopy (nsEM) was used to further evaluate

105   the conformational integrity of spike NP proteins. Imaging of spike NP revealed the forms of single

106   particles (blue circled), spike NP aggregates (yellow circled) and spike NPs with varying

107   stoichiometries (red circled), with the latter being the most predominant (Fig. 1D). The majority

108   of stoichiometries ranged from 2-9 spike proteins with one representative particle shown in Fig.

109   1D. Closer evaluation of spike proteins further validated the order and pre-fusion homogeneity of

110   the spikes on the NPs (Figs. 1E and F). Consistent with our vaccine design, these nsEM

111   observations validated that the arrangement of spike proteins on the NP sterically blocks S2

112   subunits by the proximity of adjacent spikes (Fig. 1B), and this blockage depends on the occupancy

113   rate of the spikes on the NP.

114   **In-vitro characterization and comparison of spike NP and non-NP**. Ideally, trimer mimetics

115   of the native spike on NP or by itself should present all epitopes recognized by the neutralizing

116   antibodies (nAbs). To characterize the antigenic profile of spike trimers, both spike NP and spike

117   non-NP were tested to bind to a panel of published nAbs (IgG format) targeting the RBD and

118   NTD[4,9,30,31], a non-neutralizing antibody CR3022[32] and an HIV antibody as negative control in

119   ELISAs. The binding of spike NP or non-NP to all tested IgGs were potent, with the exception of

120   the HIV antibody control (Fig. 2A). We next sought to compare the binding kinetics of two

121   representative nAbs to spike NP versus non-NP by Bio-Layer Interferometry (BLI). To eliminate

122   the multivalent binding on BLI, we first generated antibody Fab using sequences from nAbs,

123   COVA1-18 (RBD-specific) and COVA1-22 (NTD-specific)[4]. Fabs of COVA1-18 and COVA1-

124   22 were immobilized on anti-human Fab-CH1 sensors and probed with spike NP or non-NP at 7

125   different concentrations. BLI data showed that both Fabs binding to spike NP had higher affinities

126   (<pM level), compared to spike non-NP (3.54 and 0.033 nM for COVA1-18 and COV1-22 Fabs,

127   respectively), and this higher affinity to spike NP was attributed to the slower dissociation off-

128   rates (Fig. 2B). Compared to NTD-specific antibody COVA1-22 binding, the difference of binding

129   to RBD-specific antibody COVA1-18 between spike NP and non-NP was more striking (Fig. 2B),

130   suggesting that spike NP exhibits the RBD more robustly. The overall antigenic profile determined

131   by ELISA and BLI (Fig. 2) confirmed that spike NP and non-NP all displayed the favorable

132   epitopes targeted by the tested nAbs.

133   Spike NP was initially stored at -80°C. To understand the stability of spike NP stored at

134   different temperatures, we evaluated the conformational integrity and antigenicity of this protein

135   when stored at 4°C, 22°C (room temperature, RT), and 37°C for a period of 2 days, 1 week and 4

136   weeks. Three representative antibodies targeting the RBD, NTD and S2 subunits of SARS-CoV-2

137   spike protein, and a negative control antibody were used to test binding. As shown in Fig. S1, spike

138   NP stored at different temperatures for up to 4 weeks displayed binding to selected RBD and NTD-

139   specific antibodies-CB6 and 4A8[9,31] respectively, identical to positive control spike NP protein

140   stored at -80°C, although we observed slightly decreased binding to the S2 subunit-specific

141   antibody, RV82. RV82 is a fully human monoclonal antibody (IgG1) that was identified from a B

142   cell repertoire of COVID-19 convalescent human and confirmed to bind to monomeric or trimeric

143   S2 subunit proteins of SARS-CoV-2 (Fig. S2A). Consistently, RV82 retained binding to trimeric

144   spike protein of SARS-CoV-2 B.1.351 variant (initially identified in the South Africa) that has all

145   mutations located within S1 subunit, while most of tested RBD- or NTD-specific antibodies

146   showed ablated binding to these mutations, with the exception of CR3022[32] and COVA1-16[4]

147   antibodies (Left two, Fig. S2B). Different from CR3022 and COVA1-16, RV82 bound to SARS-

148   CoV-2, but not SARS (2003 strain) (Right, Fig. S2B). Together with the notion that RBD and

149   NTD are the major neutralizing epitopes[4,5,9,31], and SDS-PAGE analysis of spike NP showed no

150   difference between protein being stored at various temperatures and -80°C (data not shown), we

151   suggest that spike NP is stable up to 37°C for at least 4 weeks. In the future, other methods to

152   verify the thermostability, such as EM and DSF (Differential Scanning Fluorimetry), will be

153   utilized.

154   **Immunogenicity of spike NP and non-NP in mice.** We next evaluated the immunogenicity of

155   spike NP and non-NP in mice. Two groups of mice were immunized with spike NP and spike non-

156   NP with the Sigma Adjuvant System via subcutaneous injection route, respectively. A third group

157   of mice were injected with PBS as a negative control. We first assessed antibody binding of sera

158   collected 14- or 28-days post immunization to trimeric spike protein with D614G mutation.

159   Significant levels of spike protein-specific IgG were detected in all vaccinated mice 14 days post

160   immunization and spike NP induced spike-specific IgG ~1.5-fold higher than spike non-NP on

161   days 14 and 28, with the titer declining on day 28 (Fig. 3A). Besides trimeric spike protein binding,

162   we assessed the binding of RBD, S2, and NTD subunits to sera collected 14 days post

163   immunization. The results showed that sera from spike NP immunized mice displayed significantly

164   higher binding to RBD than sera from spike non-NP immunized animals (** $p<0.01$, Mann-

165   Whitney test) (Left, Fig. 3B), while serum binding to S2 subunit was opposite, with sera from

166   spike non-NP immunized animals showing significantly stronger binding to S2 subunit (** $p<0.01$,

167   Mann-Whitney test) (Middle, Fig. 3B), indicating NP presentation preferentially exposed RBD

168   over S2 subunit, consistent with vaccine design. NTD-specific antibody responses in all groups

169   were weak on day 14 (Right, Fig. 3B).

170   Cross-reactive and non or weak neutralizing antibodies are potentially responsible for

171   antibody-dependent enhancement (ADE). To evaluate vaccine-elicited cross-reactive antibodies,

172   we assessed sera collected on day 14 for binding to trimeric spike proteins from SARS (2003

173   strain) or MERS. Consistent with S2 subunit binding, sera from spike non-NP immunized animals

174   showed stronger binding to these two different coronavirus spike proteins than sera from spike NP

175   immunized ones, especially to the MERS spike protein (* $p<0.05$, Mann-Whitney test) (Fig. 3C).

176   The data suggested spike NP elicited less cross-reactive antibodies that are possibly S2 subunit-

177   specific.

178   Neutralizing antibodies are related to vaccine-induced protection. Sera collected on days

179   14 and 28 were tested for their neutralizing antibody activity against VSV pseudotyped virus with

180   SARS-CoV-2 spike protein containing D614G mutation and a luciferase reporter. On day 14, we

181   observed that the neutralizing antibody (nAb) titer of sera from spike NP immunized mice was on

182   average 4 log (ID_{50}), significantly higher than the titer of sera from spike non-NP immunized ones

183   (* $p<0.05$, Mann-Whitney test) (Left, Fig. 3D). Similarly, the neutralizing antibody titer declined

184   on day 28, but the titer of spike NP immunized sera was still significantly higher than that of spike

185   non-NP immunized sera (* $p<0.05$, Mann-Whitney test) (Right, Fig. 3D). To assess neutralizing

186   antibody epitope on spike protein, we analyzed the correlation between day 14 serum neutralizing

187   titer and ELISA titer obtained from either binding to spike RBD subunit or whole spike protein.

188   This analysis revealed a more correlated relationship between neutralizing titer and RBD binding

189   titer (R=0.6915, *** $p=0.0007$), compared to the correlate with spike binding (R=0.4537, *

190    $p=0.045$) (Fig. 3E), indicating RBD is the major neutralizing antibody epitope and RBD-specific

191   nAbs are responsible for serum neutralizing activity. This is in agreement with the rationale of our

192   vaccine design by using NP to preferentially present RBD, validated by the above BLI results (Fig.

193   2B).

194   **Protection efficacy of spike NP in hamsters.** Encouraged by the potent immune mouse serum

195   neutralizing antibody response elicited by spike NP that we observed on day 14, we next evaluated

196   vaccine protection efficacy in Syrian golden hamsters, one of few small animal models susceptible

197   to infection by the SARS-CoV-2 virus[33,34]. Two groups of hamsters were immunized with a single

198   dose of spike NP (REVC-128) or sham control including same NP presenting Marburg trimeric

199   GP, and same adjuvant via intramuscular injection route (Fig. 4A). We observed that sera collected

200   from spike NP immunized hamsters on day 13, one day prior to virus challenge, displayed

201   significantly higher potent neutralizing antibody activity against VSV pseudotyped with SARS-

202   CoV-2 D614G spike than sera from the sham group (* $p<0.05$, Mann-Whitney test) (Fig. 4B).

203   Fourteen days post immunization, animals were challenged with SARS-CoV-2 virus

204   intranasally. In the sham control, hamsters lost a median of 10% body weight by 7 days post

205   infection (dpi), while spike NP immunized animals gained body weight lightly from 4 dpi (Fig.

206   4C). Significant weight differences post infection were observed from 4-7 dpi (* $p<0.05$, **

207    $p<0.01$, *** $p<0.001$, two-way ANOVA test) (Fig. 4C). To determine the impact of vaccine-

208   induced immunity on tissue viral load, we measured both viral genomic and subgenomic RNA

209   amounts in lung and nares collected on 7 dpi. Viral genomic RNA (vRNA) reflects remaining viral

210   inoculum plus newly replicating virus, while subgenomic RNA (sgRNA) should only result from

211   newly replicating virus[35]. For hamsters immunized by spike NP, we observed the significantly

212   lower amounts of viral RNA in lung and nares (~3 log) than that in animal tissues in the sham

213   control (Upper, Fig. 4D). Similarly, the level of sgRNA in protected animals' tissues was

214   approximately 3 log lower than that in sham control animals' tissues (Bottom, Fig. 4D).

215   We next performed histopathology analyses of the lungs and nares of two groups of

216   infected hamsters. Qualitative and semiquantitative analyses of lung and nares tissues collected on

217   7 dpi were performed using a severity scoring scale[36,37] (Table 1). In the sham control, all hamsters

218   showed evidence of pulmonary lesions with the observations of moderate to marked bronchiolo-

219   alveolar hyperplasia (grade 3 or 4), mild mixed cell bronchiolo-alveolar inflammation (grade 2),

220   and   minimal   to   mild   mononuclear   cell   perivascular/vascular   infiltrate   or

221   alveolar/perivascular/vascular inflammation (grade 1 or 2) (Figs. 4E, F and Table 1). Perivascular

222   edema (grade 1 or 2), syncytial cells and hemorrhage (grade 1) were observed in lungs of some

223   but not all animals in the sham control (Fig. 4F and Table 1). The majority of animals in the sham

224   control also exhibited atypia of hyperplastic alveolar epithelial cells with hypertrophic and variably

225   shaped nuclei and prominent nucleoli (Fig. 4E). Syncytial cells, enlarged multinucleated cells,

226   most likely Type II pneumocytes demonstrating viral cytopathic-like changes, were scattered

227   throughout alveoli in lungs of animals in sham control. SARS-CoV-2 virus has been reported to

228   infect both Type I and Type II pneumocyte cells in animal studies[38], and the infection and loss of

229   Type I pneumocytes would contribute to the proliferation of Type II pneumocytes. Overall, the

230   histological observations in the lungs and nares of sham control were consistent with SARS-CoV-

231   2 infection reported previously[39]. In spike NP immunized animals, one animal showed minimal

232   bronchiolar hyperplasia in the lung (grade 1) and another one showed minimal lesions in nares

233   (grade 1) (Table 1), while the rest of animals in this group showed negligible histopathologic

234   phenotype.

235   In summary, weight change, viral load and histopathological data support that REVC-128

236   effectively protected against COVID-19 associated morbidity starting two weeks post a single dose

237   of immunization.

238

239   **Discussion**

240   Herein, we developed a COVID-19 protein-based nanoparticle vaccine, REVC-128.

241   Protein-based vaccines, such as the Hepatitis B vaccine that has been administered on the first day

242   of life for newborn babies, have shown minimal safety concern. The backbone of the nanoparticle,

243   ferritin, has also been shown to be safe for influenza vaccines in clinical trials. Therefore, REVC-

244   128 has the potential to protect individuals who are medically unable to receive other COVID-19

245   vaccines, such as people who are allergic to mRNA vaccines. Additionally, the vaccine stability

246   data (Fig. S1) support a much less stringent requirement for the storage of this vaccine, compared

247   with mRNA vaccines that require -20°C or -80°C storage. Vaccine storage and transportation in

248   ambient temperature condition will enable broader availability of such vaccine.

249   Vaccination using a one-dose regimen enables easier deployment, tracking and

250   administration, compared to a two-dose regimen. Further, vaccine with the capability to induce

251   early protection can more efficiently prevent viral spread and contribute to the quelling of this

252   COVID-19 pandemic. Herein, we showed that a single dose of REVC-128 provides protection

253   starting two weeks post immunization, earlier than other vaccine candidates. To our knowledge,

254   two viral vector vaccines (VSV and Ad26) have been reported to induce early protection starting

255   four weeks post immunization using a one-dose regimen[33,40], while mRNA vaccines (e.g.,

256   Moderna, Pfizer/BioNTech), inactivated vaccine (e.g., Sinovac Life Sciences) and another

257   nanoparticle protein vaccine, Novavax's NVX-CoV2373 that all use a two-dose regimen with

258   evidence of protection occurring at or after four weeks post the first dose of immunization.

259   Although viral vector vaccines induced early protection, the preexisting immunity to viral vectors

260   presents a formidable challenge for this platform, especially when a boosting immunization is

261   required. The booster enhances the immune response to viral vector, which could impair vector

262   entry into host cells. In contrast, protein or mRNA vaccines avoid this challenge and allow more

263   flexibility for multiple boosts to achieve a longer protection period or protection against mutant

264   variants. We observed the decreased neutralizing antibody titer on day 28 after a single dose of

265   immunization (Fig. 3D), and also observed the enhanced titer following a booster (data not shown).

266   The protection durability induced by both one-dose and two-dose regimens merits further

267   investigation. The immunogen dose used in this report is high (20 μg per mouse or 100 μg per

268   hamster), warranting a dose-deescalating study to assess the optimal dose in the future.

269   During this COVID-19 pandemic, concerns arose about pre-existing human coronavirus-

270   specific antibodies generated during previous infections. These antibodies may mediate antibody-

271   dependent enhancement (ADE), worsening symptoms when patients are infected with SARS-

272   CoV-2[41]. This might be one of the reasons why older adults are at higher risk for severe disease,

273   as antibodies previously generated in response to common human coronaviruses in the elderly

274   facilitate SARS-CoV-2 entrance into target cells, leading to more severe symptoms[42,43]. On the

275   contrary, seroprevalence of community-acquired coronavirus in pediatrics is not common[44]. In

276   addition, one possible explanation for SARS-CoV-2 reinfection is the antibodies induced by the

277   first infection may help, rather than fight, the second infection, which is linked to ADE[45]. Previous

278   Dengue virus vaccine studies revealed human clinical safety risk related to ADE[46], resulting in

279   vaccine trial failure. The envelope protein sequence alignment of four serotypes of Dengue and

280   Zika viruses (flavivirus family) indicates that envelope protein domain II containing fusion

281   machinery exhibits a higher degree of homology among these viruses, and virus infection induces

282   high level of domain II-specific antibodies that are non or weakly neutralizing, but responsible for

283   ADE effect[47-49]. In line with Dengue domain II, the S2 subunit of the SARS-CoV-2 spike protein

284   containing fusion machinery exhibits a higher degree of homology among coronaviruses than the

285   S1 subunit of spike protein. It has been reported that antibodies from SARS-CoV-2 naïve donors

286   who had reactivity to seasonal human coronavirus strains (such as OC43 and HKU1) were cross-

287   reactive against the nucleocapsid and S2 subunit on spike protein of SARS-CoV-2[50]. More studies

288   have reported that cross-reactive mAbs largely target this more conserved S2 subunit on spike

289   protein[51,52]. Conceptually, a number of S2 subunit-specific antibodies is non or weakly

290   neutralizing, and potentially responsible for ADE. Thus, vaccine design to minimize the elicitation

291   of S2 subunit-specific antibodies should be considered, especially when/if ADE will be observed

292   for SARS-CoV-2.

293   Although ADE has yet to be fully observed for SARS-CoV-2 infection or vaccination,

294   previous coronavirus vaccine candidates were reported to be complicated by ADE. A viral vector

295   vaccine of the original SARS was found to enhance the immunopathology of immunized animals

296   following viral challenge, resulting in a strong inflammatory response and even lung injury[53,54].

297   Mice immunized by Ad5 viral vector expressing MERS vaccine were also reported to exhibit

298   pulmonary pathology following viral challenge, despite the vaccine conferring protection[55].

299   Similar observation was reported for inactivated virus vaccine. Lung immunopathology was

300   observed when animals were immunized with inactivated whole-virus MERS vaccine, followed

301   by virus challenge[56]. One strategy to offset ADE concern of Dengue and Zika vaccines is to reduce

302   cross-reactive antibody response[57]. Similarly, we used adjacent spike proteins on NP to sterically

303   block the S2 subunit exposure, which was validated with evidence of less S2 subunit and cross-

304   reactive antibodies elicited by spike NP, compared with vaccine without NP (Figs. 3B and C). The

305   epitope mapping of these cross-reactive antibodies will be performed in the future to assess

306   whether they are S2-specific. Nevertheless, such design might prevent the development of severe

307   symptoms if patients are infected with other coronaviruses post-immunization, such as seasonal

308   coronaviruses (e.g., common cold virus), or mutated SARS-CoV-2 variants.

309

310   **Materials and Methods**

311   **Protein expression and purification.** The ectodomain (residues 1-1208) of spike protein of

312   SARS-CoV-2 was modified based on GenBank sequence of MN908947, including a glycine

313   substitution at residue 614, a "SGAG" substitution at the furin cleavage site (residues 682-685)

314   and two proline substitutions at residues 986 and 987. A C-terminal T4 fibritin trimerization motif,

315   an HRV3C protease cleavage site, an $8 \times$ His Tag and a TwinStrep Tag were conjugated with

316   ectodomain of spike protein. Ectodomain of spike protein was also conjugated with ferritin

317   nanoparticle (NP) with a linker to generate spike NP. The sequence was cloned into the mammalian

318   expression vector pCAGGS. The trimeric ectodomain of spike protein of SARS-CoV-2 South

319   African B.1.351 variant was constructed in the same way, with the exception of the following

320   mutations[58]: L18F, D80A, D215G, L242-244del, R246I, K417N, E484K, N501Y, D614G, and

321   A701V. The trimeric ectodomain of spike protein of SARS (2003 strain) was modified based on

322   GenBank sequence of AY278554, including two proline substitutions at residues 968 and 969[59],

323   same trimerization motif, HRV3C cleavage site and tags. The trimeric ectodomain of spike protein

324   of MERS was modified based on GenBank sequence of JX869059, including furin cleavage site

325   knockout, two proline substitutions at residues 1060 and 1061[60], same trimerization motif, HRV3C

326   cleavage site and tags.

327   To express trimeric S2 subunit of spike protein, residues 686-1208 of SARS-CoV-2 were

328   cloned upstream of a C-terminal T4 fibritin trimerization motif, an HRV3C protease cleavage site,

329   an $8 \times$ His Tag and a TwinStrep Tag. Residues 319-541 of SARS-CoV-2 were cloned with C-

330   terminal $6 \times$ His Tag for RBD. Similarly, residues 14-305 of SARS-CoV-2 were cloned with C-

331   terminal $6 \times$ His Tag for NTD.

332   These expression vectors were codon optimized and confirmed by sequencing prior to

333   being transiently transfected into FreeStyle™ 293F cells (Thermo Fisher). Protein was purified

334   from filtered cell supernatants using StrepTactin resin (IBA) or cOmplete His-Tag Purification

335   Resin (Roche) or Jacalin (Thermo Fisher). The purified protein was subjected to additional

336   purification or analysis by size-exclusion chromatography using a Superose 6 column.

337   Plasmids encoding the heavy and light chains of CR3022, COVA1-16, COVA1-18,

338   COVA1-22, B38, CA1, CB6, H4, 4A8 and RV82 in a human IgG1 expression vector[61,62] were

339   transiently transfected into FreeStyle™ 293F cells and purified as described previously[62,63]. To

340   express antibody Fab, the heavy chain variable domain was inserted into Fab expression vector

341   containing a $6 \times$ His Tag as previously described[63], followed by co-transfection with light chain

342   expression vector. Fab was purified from cell culture supernatant by cOmplete His-Tag

343   Purification Resin (Roche).

344   **ELISA binding assays.** Proteins of trimeric spikes of SARS, MERS, or SARS-CoV-2 or RBD,

345   NTD and S2 subunits of SARS-CoV-2 were coated onto 96-well Maxisorb ELISA plates at 200

346   ng/well diluted in PBS overnight at 4°C. On the following day, the plates were washed four times

347   with 300 μL of $1 \times$ PBST (0.05% Tween-20) and blocked with blocking buffer (2% dry milk / 5%

348   fetal bovine serum in PBS) for 1 hour at 37°C. After blocking, plates were washed as described

349   above prior to adding mAbs diluted into same blocking buffer starting from 10 μg/ml or heat-

350   inactivated animal serum starting from 100-fold dilution with 5-fold serial dilutions for 1 hour at

351   37°C. After incubation, plates were washed and a 1: 5,000 dilution of Goat anti-human or anti-

352   mouse IgG-HRP conjugate (Jackson ImmunoResearch) in PBST was added for 1 hour at room

353   temperature. The bound mAb was detected with adding 100 μl/well of 3,3′,5,5′-

354   Tetramethylbenzidine (TMB) substrate (Life Technologies) and incubation at room temperature

355   for 5 min prior to the addition of 100 μl of 3% H_2SO_4 to stop the reaction. The optical density

356   (OD) was measured at 450 nm.

357 **BioLayer interferometry.** Biolayer light interferometry (BLI) was performed using an Octet

358 RED96 instrument (ForteBio, Pall Life Sciences) as described previously[62-64]. Antibody Fab was

359 captured onto anti-human Fab-CH1 biosensors at concentration of 10 μg/ml as ligand and the

360 tested samples of spike NP or non-NP was diluted in 7×2-fold series starting from 250 nM to 3.9

361 nM in solution, respectively. Briefly, biosensors, pre-hydrated in binding buffer ($1\times$ PBS, 0.01%

362 BSA and 0.2% Tween-20) for 10 min were first immersed in binding buffer for 60 s to establish a

363 baseline followed by submerging in a solution containing ligand for 60 s to capture ligand. The

364 biosensors were then submerged in binding buffer for a wash for 60 s. The biosensors were then

365 immersed in a solution containing various concentrations of tested samples as analyte for 120 s to

366 detect analyte/ligand association, followed by 120 s in binding buffer to assess analyte/ligand

367 dissociation. Binding affinity constants (dissociation constant, K_D; on-rate, k_{on}; off-rate, k_{off}) were

368 determined using Octet Analysis software.

369 **VSV-spike pseudovirus production and neutralization assay.** To generate SARS-CoV-2 spike

370 VSV pseudovirus, a plasmid encoding SARS-CoV-2 spike harboring a C-terminal 18-residue

371 truncation was transfected into pre-seeded 293T cells. Next day, transfected cells were infected

372 with VSV(G*ΔG-luciferase) (Kerafast) at an MOI of 3 infectious units/cell. The cell supernatant

373 containing SARS-CoV-2 pseudotyped VSV was collected at day 2 post-transfection, centrifuged

374 to remove cellular debris, aliquoted and frozen at -80°C.

375 Neutralization assays using above SARS-CoV-2 pseudotyped VSV were performed as

376 previously described[65] with modification. This pseudovirus was first titrated with duplicate on

377 Vero E6 cells cultured in EMEM supplemented with 10% fetal bovine serum and 100 I.U./mL

378 penicillin and 100 μg/mL streptomycin at 37°C. The dilution of pseudovirus to achieve 1,000-fold

379 luciferase signal higher than background was selected for neutralization assay. In neutralization

380   assay, the heat-inactivated serum starting from 100-fold dilution with serial dilutions was

381   incubated with diluted pseudotyped virus in EMEM for 1 hour at 37°C before infecting Vero E6

382   cells at 37°C, 5% CO_2 for 1 hour. The next day, cells were lysed with Passive Lysis Buffer

383   (Promega) for 40 minutes at room temperature with shaking before the addition of the Luciferase

384   Activating Reagent (Promega). The luminesce was read immediately on a Molecular Devices

385   reader. Percent neutralization was calculated based on wells containing virus only and cells only

386   as background. Data was fit to a 4PL curve in GraphPad Prism 7.

387   **Negative stain Electron microscopy.** Negative stain electron microscopy (nsEM) was performed

388   as previously described[65,66]. Briefly, spike NP was added to 400 square copper mesh grids coated

389   with carbon and stained with 2% uranyl formate. The grids were imaged on a 120keV Tecnai Spirit

390   electron microscope using an Eagle 4k × 4k CCD camera. NP particles were manually selected

391   from the raw micrograph stacked with a box size of 200 pixels and aligned using iterative

392   MRA/MSA[67]. Single particles were picked with DogPicker and processed in RELION 3.0.

393   **Animal experiments.** Animal experiments were carried out in compliance with all pertinent US

394   National Institutes of Health regulations and approval from the Animal Care and Use Committee

395   (ACUC) of Noble Life Sciences and Bioqual. For the immunogenicity study, 6-to 8-week-old

396   female C57BL/6 mice (Jackson Laboratory) were inoculated subcutaneously in two sites. Each

397   animal received a single dose of 20 μg protein immunogen in 100 μl of PBS containing 50 μl of

398   Sigma Adjuvant System (Sigma) with the procedure of immunogen and adjuvant mixture

399   following manufacture's manual. For serum preparation, blood samples were collected retro-

400   orbitally on days 0, 14 and 28. For the protection efficacy study conducted at Bioqual, 7-week-old

401   male and female Syrian golden hamsters were inoculated intramuscularly into each hind leg. Each

402   animal received a single dose of 100 μg protein immunogen in 200 μl of PBS containing 100 μl

403   of the same adjuvant. For serum preparation, blood samples were collected retro-orbitally on days

404   0 and 13. On day 14, all animals were challenged with 1.99×10^4 TCID$_{50}$ of SARS-CoV-2 virus

405   (USA-WA1/2020, NR-53780 BEI Resources). Virus was administered as 100 µl by the intranasal

406   route (50 µl into each nostril). Body weights were assessed daily. All animals were sacrificed on

407   7 dpi for tissue analyses. Challenge studies were conducted under maximum containment in an

408   animal biosafety level 3 facility under ACUC-approved protocol in compliance with the Animal

409   Welfare Act and other federal statutes and regulations relating to animals and experiments

410   involving animals.

411   **Quantitative RT-PCR assay for SARS-CoV-2 RNA**

412   The amounts of RNA copies per gram tissue were measured using a qRT-PCR assay as described

413   previously[34]. Briefly, viral RNA was extracted from lung and nares collected on 7 dpi with RNA-

414   STAT 60 (Tel-test"B")/chloroform, precipitated and resuspended in AVE Buffer (Qiagen). To

415   generate a control for the amplification reaction, RNA was isolated from the applicable virus stock

416   using the same procedure. RT-PCR assays were performed using TaqMan RT-PCR kit (Bioline,

417   BIO-78005) with primers and probe sequences described previously[34]. The signal was compared

418   to the known standard curve and calculated to give copies per gram (g). All samples were tested

419   in triplicate.

420   **Quantitative RT-PCR assay for SARS-CoV-2 subgenomic RNA**

421   SARS-CoV-2 subgenomic mRNA (sgRNA) was determined as described previously[34] with

422   modification. Briefly, above extracted RNA was first reverse-transcribed using Superscript III

423   VILO (Invitrogen) according to the manufacturer's instructions. A Taqman custom gene

424   expression assay (ThermoFisher Scientific) was designed using the sequences targeting the N gene

425   sgRNA. Reactions were performed on a QuantStudio 6 and 7 Flex Real-Time PCR System

426   (Applied Biosystems) with following primers and probe sequences. Standard curves generated

427   using SARS-CoV-2 N gene sgRNA pre-cloned into an expression plasmid were used to calculate

428   sgRNA in copies per gram. All samples were tested in triplicate.

429   Subgenomic RNA primers:

430   SG-N-F: CGATCTCTTGTAGATCTGTTCTC

431   SG-N-R: GGTGAACCAAGACGCAGTAT

432   Probe: FAM/TAACCAGAA/ZEN/TGGAGAACGCAGTGGG/IABkFQ

433   **Histopathology**. Hamsters were euthanized for necropsy on 7 dpi. Lung and nares were collected

434   in 10% neutral buffered formalin (NBF), followed by being fixed, processed to hematoxylin and

435   eosin (H&E) stained slides and examined by a board-certified pathologist. Qualitative and

436   semiquantitative assessment were performed as described previously[36,37], industry best practices[68]

437   and terminology for data capture were consistent with International Harmonization of

438   Nomenclature and Diagnostic Criteria (INHAND)[69,70].

439   **Statistical analysis.** ELISA, nAb titer or viral load statistical analyses of comparison between

440   spike NP and non-NP or sham immunized animal sera were performed by using the Mann-Whitney

441   test with * $p<0.05$, ** $p<0.01$. Correlation statistical analyses between ELISA and nAb titers were

442   performed by using the Spearman nonparametric test with * $p<0.05$, *** $p<0.001$. The statistical

443   analysis of comparison of body weight change at each time point between animals with spike NP

444   and mock immunized was performed by using the two-way ANOVA test with * $p<0.05$, ** $p<0.01$,

445   *** $p<0.001$ using GraphPad Prism version 8.

446

447   **Acknowledgments**

References

461   1   Cheng, Z. J. & Shan, J. 2019 Novel coronavirus: where we are and what we know.
462   *Infection* **48**, 155-163, doi:10.1007/s15010-020-01401-y (2020).
463   2   Walls, A. C. *et al.* Cryo-electron microscopy structure of a coronavirus spike glycoprotein
464   trimer. *Nature* **531**, 114-117, doi:10.1038/nature16988 (2016).
465   3   Walls, A. C. *et al.* Tectonic conformational changes of a coronavirus spike glycoprotein
466   promote membrane fusion. *Proc Natl Acad Sci U S A* **114**, 11157-11162,
467   doi:10.1073/pnas.1708727114 (2017).
468   4   Brouwer, P. J. M. *et al.* Potent neutralizing antibodies from COVID-19 patients define
469   multiple targets of vulnerability. *Science* **369**, 643-650, doi:10.1126/science.abc5902
470   (2020).
471   5   Rogers, T. F. *et al.* Isolation of potent SARS-CoV-2 neutralizing antibodies and protection
472   from disease in a small animal model. *Science* **369**, 956-963,
473   doi:10.1126/science.abc7520 (2020).
474   6   Wec, A. Z. *et al.* Broad neutralization of SARS-related viruses by human monoclonal
475   antibodies. *Science* **369**, 731-736, doi:10.1126/science.abc7424 (2020).
476   7   Robbiani, D. F. *et al.* Convergent antibody responses to SARS-CoV-2 in convalescent
477   individuals. *Nature* **584**, 437-442, doi:10.1038/s41586-020-2456-9 (2020).
478   8   Hansen, J. *et al.* Studies in humanized mice and convalescent humans yield a SARS-CoV-
479   2 antibody cocktail. *Science* **369**, 1010-1014, doi:10.1126/science.abd0827 (2020).

480   9   Chi, X. *et al.* A neutralizing human antibody binds to the N-terminal domain of the Spike
481   protein of SARS-CoV-2. *Science* **369**, 650-655, doi:10.1126/science.abc6952 (2020).
482   10   Slifka, M. K. & Amanna, I. J. Role of Multivalency and Antigenic Threshold in Generating
483   Protective Antibody Responses. *Front Immunol* **10**, 956, doi:10.3389/fimmu.2019.00956
484   (2019).
485   11   Chattopadhyay, S., Chen, J. Y., Chen, H. W. & Hu, C. J. Nanoparticle Vaccines Adopting
486   Virus-like Features for Enhanced Immune Potentiation. *Nanotheranostics* **1**, 244-260,
487   doi:10.7150/ntno.19796 (2017).
488   12   Schiller, J. & Lowy, D. Explanations for the high potency of HPV prophylactic vaccines.
489   *Vaccine* **36**, 4768-4773, doi:10.1016/j.vaccine.2017.12.079 (2018).
490   13   Burton, D. R. Advancing an HIV vaccine; advancing vaccinology. *Nat Rev Immunol* **19**, 77-
491   78, doi:10.1038/s41577-018-0103-6 (2019).
492   14   Jardine, J. G. *et al.* HIV-1 broadly neutralizing antibody precursor B cells revealed by
493   germline-targeting immunogen. *Science* **351**, 1458-1463, doi:10.1126/science.aad9195
494   (2016).
495   15   Brouwer, P. J. M. *et al.* Two-component spike nanoparticle vaccine protects macaques
496   from SARS-CoV-2 infection. *Cell* **184**, 1188-1200 e1119, doi:10.1016/j.cell.2021.01.035
497   (2021).
498   16   Walls, A. C. *et al.* Elicitation of Potent Neutralizing Antibody Responses by Designed
499   Protein Nanoparticle Vaccines for SARS-CoV-2. *Cell* **183**, 1367-1382 e1317,
500   doi:10.1016/j.cell.2020.10.043 (2020).
501   17   Tian, J. H. *et al.* SARS-CoV-2 spike glycoprotein vaccine candidate NVX-CoV2373
502   immunogenicity in baboons and protection in mice. *Nat Commun* **12**, 372,
503   doi:10.1038/s41467-020-20653-8 (2021).
504   18   Guebre-Xabier, M. *et al.* NVX-CoV2373 vaccine protects cynomolgus macaque upper
505   and lower airways against SARS-CoV-2 challenge. *Vaccine* **38**, 7892-7896,
506   doi:10.1016/j.vaccine.2020.10.064 (2020).
507   19   Yassine, H. M. *et al.* Hemagglutinin-stem nanoparticles generate heterosubtypic
508   influenza protection. *Nat Med* **21**, 1065-1070, doi:10.1038/nm.3927 (2015).
509   20   Kanekiyo, M. *et al.* Self-assembling influenza nanoparticle vaccines elicit broadly
510   neutralizing H1N1 antibodies. *Nature* **499**, 102-106, doi:10.1038/nature12202 (2013).
511   21   He, L. *et al.* Approaching rational epitope vaccine design for hepatitis C virus with meta-
512   server and multivalent scaffolding. *Sci Rep* **5**, 12501, doi:10.1038/srep12501 (2015).
513   22   Sliepen, K. *et al.* Presenting native-like HIV-1 envelope trimers on ferritin nanoparticles
514   improves their immunogenicity. *Retrovirology* **12**, 82, doi:10.1186/s12977-015-0210-4
515   (2015).
516   23   He, L. *et al.* Presenting native-like trimeric HIV-1 antigens with self-assembling
517   nanoparticles. *Nat Commun* **7**, 12041, doi:10.1038/ncomms12041 (2016).
518   24   Kanekiyo, M. *et al.* Rational Design of an Epstein-Barr Virus Vaccine Targeting the
519   Receptor-Binding Site. *Cell* **162**, 1090-1100, doi:10.1016/j.cell.2015.07.043 (2015).
520   25   Powell, A. E. *et al.* A single immunization with spike-functionalized ferritin vaccines
521   elicits neutralizing antibody responses against SARS-CoV-2 in mice. *bioRxiv*,
522   doi:10.1101/2020.08.28.272518 (2020).

523   26   Zhang, L. *et al.* SARS-CoV-2 spike-protein D614G mutation increases virion spike density
524   and infectivity. *Nature Communications* **11**, 6013, doi:10.1038/s41467-020-19808-4
525   (2020).
526   27   Plante, J. A. *et al.* Spike mutation D614G alters SARS-CoV-2 fitness. *Nature*,
527   doi:10.1038/s41586-020-2895-3 (2020).
528   28   Korber, B. *et al.* Tracking Changes in SARS-CoV-2 Spike: Evidence that D614G Increases
529   Infectivity of the COVID-19 Virus. *Cell* **182**, 812-827 e819, doi:10.1016/j.cell.2020.06.043
530   (2020).
531   29   Wrapp, D. *et al.* Cryo-EM structure of the 2019-nCoV spike in the prefusion
532   conformation. *Science* **367**, 1260-1263, doi:10.1126/science.abb2507 (2020).
533   30   Wu, Y. *et al.* A noncompeting pair of human neutralizing antibodies block COVID-19
534   virus binding to its receptor ACE2. *Science* **368**, 1274-1278, doi:10.1126/science.abc2241
535   (2020).
536   31   Shi, R. *et al.* A human neutralizing antibody targets the receptor-binding site of SARS-
537   CoV-2. *Nature* **584**, 120-124, doi:10.1038/s41586-020-2381-y (2020).
538   32   ter Meulen, J. *et al.* Human monoclonal antibody combination against SARS coronavirus:
539   synergy and coverage of escape mutants. *PLoS Med* **3**, e237,
540   doi:10.1371/journal.pmed.0030237 (2006).
541   33   Tostanoski, L. H. *et al.* Ad26 vaccine protects against SARS-CoV-2 severe clinical disease
542   in hamsters. *Nat Med* **26**, 1694-1700, doi:10.1038/s41591-020-1070-6 (2020).
543   34   Baum, A. *et al.* REGN-COV2 antibodies prevent and treat SARS-CoV-2 infection in rhesus
544   macaques and hamsters. *Science* **370**, 1110-1115, doi:10.1126/science.abe2402 (2020).
545   35   Chandrashekar, A. *et al.* SARS-CoV-2 infection protects against rechallenge in rhesus
546   macaques. *Science* **369**, 812-817, doi:10.1126/science.abc4776 (2020).
547   36   Shackelford, C., Long, G., Wolf, J., Okerberg, C. & Herbert, R. Qualitative and
548   quantitative analysis of nonneoplastic lesions in toxicology studies. *Toxicologic*
549   *pathology* **30**, 93-96, doi:10.1080/01926230252824761 (2002).
550   37   Schafer, K. A. *et al.* Use of Severity Grades to Characterize Histopathologic Changes.
551   *Toxicologic pathology* **46**, 256-265, doi:10.1177/0192623318761348 (2018).
552   38   Mason, R. J. Pathogenesis of COVID-19 from a cell biology perspective. *Eur Respir J* **55**,
553   doi:10.1183/13993003.00607-2020 (2020).
554   39   Sia, S. F. *et al.* Pathogenesis and transmission of SARS-CoV-2 in golden hamsters. *Nature*
555   **583**, 834-838, doi:10.1038/s41586-020-2342-5 (2020).
556   40   Yahalom-Ronen, Y. *et al.* A single dose of recombinant VSV-G-spike vaccine provides
557   protection against SARS-CoV-2 challenge. *Nat Commun* **11**, 6402, doi:10.1038/s41467-
558   020-20228-7 (2020).
559   41   Tetro, J. A. Is COVID-19 receiving ADE from other coronaviruses? *Microbes Infect* **22**, 72-
560   73, doi:10.1016/j.micinf.2020.02.006 (2020).
561   42   Gorse, G. J., Patel, G. B., Vitale, J. N. & O'Connor, T. Z. Prevalence of antibodies to four
562   human coronaviruses is lower in nasal secretions than in serum. *Clin Vaccine Immunol*
563   **17**, 1875-1880, doi:10.1128/CVI.00278-10 (2010).
564   43   Kang, S. J. & Jung, S. I. Age-Related Morbidity and Mortality among Patients with COVID-
565   19. *Infect Chemother* **52**, 154-164, doi:10.3947/ic.2020.52.2.154 (2020).

566   44   Prill, M. M. *et al.* Human coronavirus in young children hospitalized for acute respiratory
567   illness and asymptomatic controls. *Pediatr Infect Dis J* **31**, 235-240,
568   doi:10.1097/INF.0b013e31823e07fe (2012).
569   45   Ledford, H. Coronavirus reinfections: three questions scientists are asking. *Nature* **585**,
570   168-169, doi:10.1038/d41586-020-02506-y (2020).
571   46   Sridhar, S. *et al.* Effect of Dengue Serostatus on Dengue Vaccine Safety and Efficacy. *N
572   Engl J Med* **379**, 327-340, doi:10.1056/NEJMoa1800820 (2018).
573   47   Richner, J. M. *et al.* Modified mRNA Vaccines Protect against Zika Virus Infection. *Cell*
574   **169**, 176, doi:10.1016/j.cell.2017.03.016 (2017).
575   48   Kawiecki, A. B. & Christofferson, R. C. Zika Virus-Induced Antibody Response Enhances
576   Dengue Virus Serotype 2 Replication In Vitro. *J Infect Dis* **214**, 1357-1360,
577   doi:10.1093/infdis/jiw377 (2016).
578   49   Stettler, K. *et al.* Specificity, cross-reactivity, and function of antibodies elicited by Zika
579   virus infection. *Science* **353**, 823-826, doi:10.1126/science.aaf8505 (2016).
580   50   Khan, S. *et al.* Analysis of Serologic Cross-Reactivity Between Common Human
581   Coronaviruses and SARS-CoV-2 Using Coronavirus Antigen Microarray. *bioRxiv*,
582   doi:10.1101/2020.03.24.006544 (2020).
583   51   Song, G. *et al.* Cross-reactive serum and memory B cell responses to spike protein in
584   SARS-CoV-2 and endemic coronavirus infection. *bioRxiv*,
585   doi:10.1101/2020.09.22.308965 (2020).
586   52   Cohen, S. A., Kellogg, C. & Equils, O. Neutralizing and cross-reacting antibodies:
587   implications for immunotherapy and SARS-CoV-2 vaccine development. *Hum Vaccin
588   Immunother*, 1-4, doi:10.1080/21645515.2020.1787074 (2020).
589   53   Weingartl, H. *et al.* Immunization with modified vaccinia virus Ankara-based
590   recombinant vaccine against severe acute respiratory syndrome is associated with
591   enhanced hepatitis in ferrets. *J Virol* **78**, 12672-12676, doi:10.1128/JVI.78.22.12672-
592   12676.2004 (2004).
593   54   Liu, L. *et al.* Anti-spike IgG causes severe acute lung injury by skewing macrophage
594   responses during acute SARS-CoV infection. *JCI Insight* **4**, doi:10.1172/jci.insight.123158
595   (2019).
596   55   Hashem, A. M. *et al.* A Highly Immunogenic, Protective, and Safe Adenovirus-Based
597   Vaccine Expressing Middle East Respiratory Syndrome Coronavirus S1-CD40L Fusion
598   Protein in a Transgenic Human Dipeptidyl Peptidase 4 Mouse Model. *J Infect Dis* **220**,
599   1558-1567, doi:10.1093/infdis/jiz137 (2019).
600   56   Agrawal, A. S. *et al.* Immunization with inactivated Middle East Respiratory Syndrome
601   coronavirus vaccine leads to lung immunopathology on challenge with live virus. *Hum
602   Vaccin Immunother* **12**, 2351-2356, doi:10.1080/21645515.2016.1177688 (2016).
603   57   Richner, J. M. *et al.* Modified mRNA Vaccines Protect against Zika Virus Infection. *Cell*
604   **168**, 1114-1125 e1110, doi:10.1016/j.cell.2017.02.017 (2017).
605   58   Wu, K. *et al.* mRNA-1273 vaccine induces neutralizing antibodies against spike mutants
606   from global SARS-CoV-2 variants. *bioRxiv*, doi:10.1101/2021.01.25.427948 (2021).
607   59   Kirchdoerfer, R. N. *et al.* Stabilized coronavirus spikes are resistant to conformational
608   changes induced by receptor recognition or proteolysis. *Sci Rep* **8**, 15701,
609   doi:10.1038/s41598-018-34171-7 (2018).

610	60	Pallesen, J. *et al.* Immunogenicity and structures of a rationally designed prefusion MERS-CoV spike antigen. *Proc Natl Acad Sci U S A* **114**, E7348-E7357, doi:10.1073/pnas.1707304114 (2017).
613	61	Tiller, T. *et al.* Efficient generation of monoclonal antibodies from single human B cells by single cell RT-PCR and expression vector cloning. *J Immunol Methods* **329**, 112-124, doi:10.1016/j.jim.2007.09.017 (2008).
616	62	Wang, Y. *et al.* High-Resolution Longitudinal Study of HIV-1 Env Vaccine-Elicited B Cell Responses to the Virus Primary Receptor Binding Site Reveals Affinity Maturation and Clonal Persistence. *J Immunol* **196**, 3729-3743, doi:10.4049/jimmunol.1502543 (2016).
619	63	Wang, Y. *et al.* HIV-1 Cross-Reactive Primary Virus Neutralizing Antibody Response Elicited by Immunization in Nonhuman Primates. *J Virol* **91**, e00910-00917, doi:10.1128/JVI.00910-17 (2017).
622	64	Zhao, X. *et al.* Immunization-Elicited Broadly Protective Antibody Reveals Ebolavirus Fusion Loop as a Site of Vulnerability. *Cell* **169**, 891-904 e815, doi:10.1016/j.cell.2017.04.038 (2017).
625	65	Wang, Y. e. a. Prominent Neutralizing Antibody Response Targeting the Ebolavirus Glycoprotein Subunit Interface Elicited by Immunization. *Journal of Virology* **in print** (2021).
628	66	Bangaru, S. *et al.* Structural analysis of full-length SARS-CoV-2 spike protein from an advanced vaccine candidate. *Science* **370**, 1089-1094, doi:10.1126/science.abe1502 (2020).
631	67	Ogura, T., Iwasaki, K. & Sato, C. Topology representing network enables highly accurate classification of protein images taken by cryo electron-microscope without masking. *J Struct Biol* **143**, 185-200 (2003).
634	68	Crissman, J. W. *et al.* Best practices guideline: toxicologic histopathology. *Toxicologic pathology* **32**, 126-131, doi:10.1080/01926230490268756 (2004).
636	69	Mann, P. C. *et al.* International harmonization of toxicologic pathology nomenclature: an overview and review of basic principles. *Toxicologic pathology* **40**, 7s-13s, doi:10.1177/0192623312438738 (2012).
639	70	Renne, R. *et al.* Proliferative and nonproliferative lesions of the rat and mouse respiratory tract. *Toxicologic pathology* **37**, 5s-73s, doi:10.1177/0192623309353423 (2009).
642		

643 **Table 1. Macroscopic observation of lung and nares from spike NP immunized and sham control on**

644 **7 dpi**

Microscopic observation and grading	Immunogen	Spike NP				Sham			
	Animal individual	753	754	755	756	757	758	759	760
	Gender	F	F	M	M	F	F	M	M
Lung									
Edema, vascular/perivascular, grade 1						■		■	
Edema, vascular/perivascular, grade 2							■		
Hemorrhage, alveolar, grade 1								■	
Hyperplasia, bronchiolar, grade 1				■					
Hyperplasia, bronchiolo-alveolar, grade 3								■	
Hyperplasia, bronchiolo-alveolar, grade 4						■			■
Hypertrophy, mesothelium, grade 1									■
Inflammation, mixed cell, alveolar, grade 2						■	■	■	■
Infiltrate, mononuclear cell, vascular/perivascular, grade 1									■
Inflammation, mononuclear cell, vascular/perivascular, grade 1						■		■	
Inflammation, mononuclear cell, vascular/perivascular, grade 2							■		
Mineralization, grade 1									■
Syncytial cell, present						■		■	
Nares									
Cell debris, lumen, grade 1						■		■	
Infiltrate, neutrophil, mucosa, grade 1		n/a ■					■		

645 Notes: Red and white background indicates observed and non-observed lesions, respectively. Nares/nasal
646 turbinate is missing in animal 753.
647
648   **Severity Grading Scale**
649
650 The severity of the non-neoplastic tissue lesions is graded as follows:
651
652 **Grade 1 (1+): <u>Minimal.</u>** This corresponds to a histopathologic change ranging from inconspicuous to
653 barely noticeable but so minor, small, or infrequent as to warrant no more than the least assignable grade.
654 For multifocal or diffusely-distributed lesions, this grade was used for processes where less than
655 approximately10% of the tissue in an average high-power field was involved. For focal or diffuse
656 hyperplastic/hypoplastic/ atrophic lesions, this grade was used when the affected structure or tissue had
657 undergone a less than approximately 10% increase or decrease in volume.
658
659 **Grade 2 (2+) <u>Mild.</u>** This corresponds to a histopathologic change that is a noticeable but not a prominent
660 feature of the tissue. For multifocal or diffusely-distributed lesions, this grade was used for processes where
661 between approximately 10% and 25% of the tissue in an average high-power field was involved. For focal
662 or diffuse hyperplastic/hypoplastic/atrophic lesions, this grade was used when the affected structure or
663 tissue had undergone between an approximately 10% to 25% increase or decrease in volume.
664
665 **Grade 3 (3+): <u>Moderate.</u>** This corresponds to a histopathologic change that is a prominent but not a
666 dominant feature of the tissue. For multifocal or diffusely-distributed lesions, this grade was used for
667 processes where between approximately 25% and 50% of the tissue in an average high-power field was
668 involved. For focal or diffuse hyperplastic/hypoplastic/atrophic lesions, this grade was used when the
669 affected structure or tissue had undergone between an approximately 25% to 50% increase or decrease in
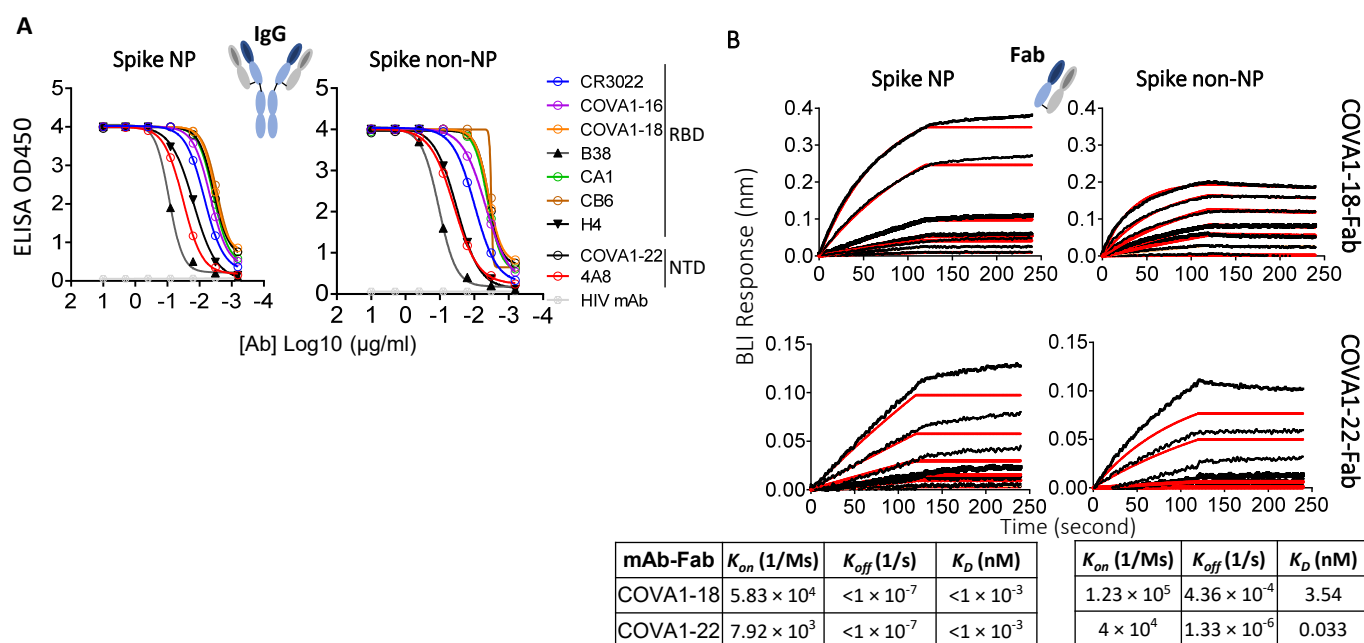670 volume.

671

672 **Grade 4 (4+): <u>Marked</u>.** This corresponds to a histopathologic change that is a dominant but not an
673 overwhelming feature of the tissue. For multifocal or diffusely-distributed lesions, this grade was used for
674 processes where between approximately 50% and 95% of the tissue in an average high-power field was
675 involved. For focal or diffuse hyperplastic/hypoplastic/atrophic lesions, this grade was used when the
676 affected structure or tissue had undergone between an approximately 50% to 95% increase or decrease in
677 volume.

678

679 **Grade 5 (5+): <u>Severe</u>.** This corresponds to a histopathologic change that is an overwhelming feature of
680 the tissue. For multifocal or diffusely-distributed lesions, this grade was used for processes where greater
681 than approximately 95% of the tissue in an average high-power field was involved. For focal or diffuse
682 hyperplastic/hypoplastic/atrophic lesions, this grade was used when the affected structure or tissue had
683 undergone a greater than approximately 95% increase of decrease in volume.
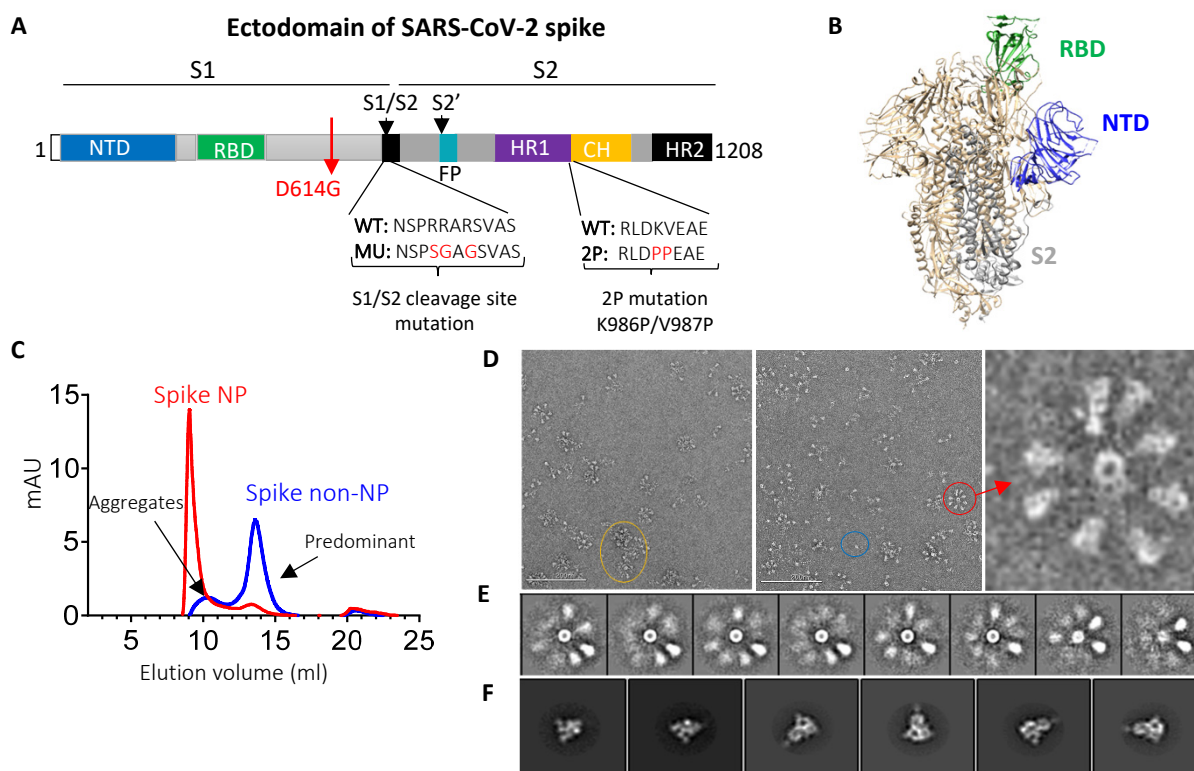
Figure 1. **SARS-CoV-2 spike ectodomain and nanoparticle presenting trimeric spike ectodomain**. (**A**) Schematic of SARS-CoV-2 spike protein ectodomain. NTD: N-terminal domain; RBD: receptor-binding domain; S1/S2= S1/S2 protease cleavage site; FP= fusion peptide; HR= heptad repeat. Two arrows indicate the cleavage sites. The native furin cleavage site was knocked out (RRAR→SGAG), two proline at positions K986 and V987 substituted, and one glycine at position D614 substituted for ectodomain expression and nanoparticle conjugation. (**B**) Schematic of prefusion conformation of SARS-Cov-2 trimeric S structure with NTD, RBD and S2 subunit highlighted in blue, green and grey on one protomer, respectively (PDB:6VSB). (**C**) Size-exclusion chromatography (SEC) profiles of spike NP (red) and spike non-NP (blue) presentation on a Superose 6 column. (**D**) Spike NP observation by negative stain EM. In the raw micrograph, the representative of nanoparticle single particle, spike NP aggregates and NPs with varying stoichiometries was circled in blue, yellow and red, respectively. The closer observation of a selected multivalent spike NP is on the right. The grey scale bar represents 200 nm. (**E**) 2D classes averages of spike NP. The pictures show varying numbers of spike proteins on NPs. (**F**) Spike trimers are in the desired prefusion conformation on NP.

mAb-Fab	K_{on} (1/Ms)	K_{off} (1/s)	K_D (nM)	K_{on} (1/Ms)	K_{off} (1/s)	K_D (nM)
COVA1-18	5.83×10^4	$<1 \times 10^{-7}$	$<1 \times 10^{-3}$	1.23×10^5	4.36×10^{-4}	3.54
COVA1-22	7.92×10^3	$<1 \times 10^{-7}$	$<1 \times 10^{-3}$	4×10^4	1.33×10^{-6}	0.033

Figure 2. **Characterize and compare antigenicity of spike NP and spike non-NP.** (**A**) Antibody (IgG format) binding to spike NP protein (left) and spike non-NP (right) in ELISAs with raw curves displayed. Antibodies targeting RBD and NTD were indicated with a control HIV antibody. (**B**) Kinetics of antibody Fab-spike binding characterization by Bio-Layer Interferometry (BLI). BLI curves were generated with two published antibody Fab format COVA1-18 on the top and COVA1-22 at the bottom, immobilized on anti-human Fab-CH1 sensors, followed by probing with spike NP or non-NP proteins at concentrations of 250, 125, 62.5, 31.3, 15.6, 7.8 and 3.9 nM. Raw and fit curves were labeled in black and red, respectively. Binding kinetic measurements were indicated below the sensograms.
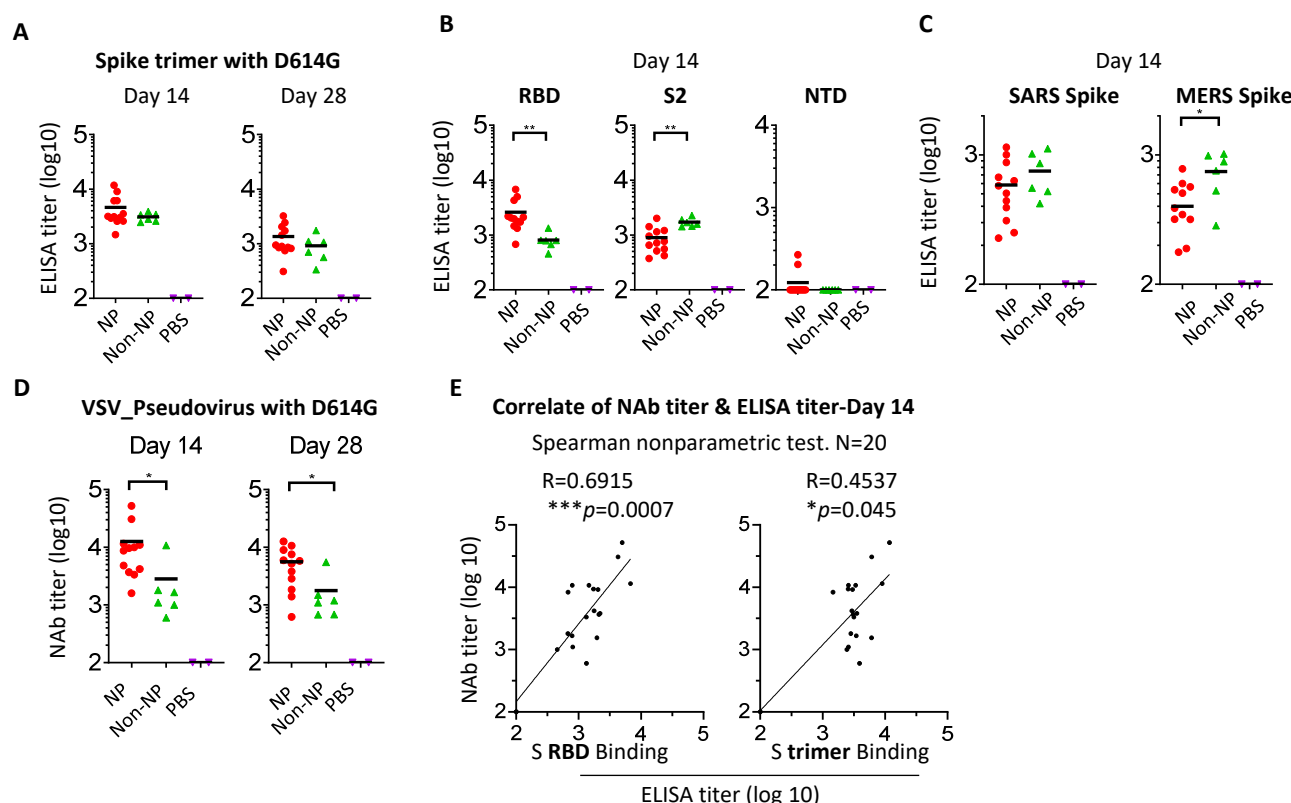
Figure 3. **Immune response to spike NP or non-NP**. (**A**) Wide-type C57BL/6 mice were immunized with 20 μg spike NP or spike non-NP with Sigma Adjuvant System via subcutaneous injection route. The serum was collected 14- and 28-days post immunization and tested to bind to SARS-CoV-2 spike trimeric protein with D614G mutation in ELISAs. ELISA titer was calculated on reciprocal serum dilution to achieve 50% of maximal optical absorbance (OD). Black bars reflect mean responses. (**B**) The binding of sera collected at day 14 to spike RBD, S2 and NTD subunits of SARS-CoV-2 in ELISAs. Statistical analysis was performed with Mann-Whitney test (** $p<0.01$). (**C**) The binding of sera collected at day 14 to trimeric spike protein of SARS (2003 strain) and MERS. Statistical analysis was performed with Mann-Whitney test (* $p<0.05$). (**D**) The neutralizing activity of sera collected at days 14 and 28 against VSV pseudotyped virus with SARS-CoV-2 spike protein containing D614G mutation. NAb titer (neutralizing antibody) represents the reciprocal of the antiserum dilution at which virus entry is inhibited by 50%, when calculated after curve-fitting with the Prism program (GraphPad). Black bars reflect mean responses. Statistical analysis was performed with Mann-Whitney test (* $p<0.05$). (**E**) The correlate of serum neutralizing titer and ELISA titer of binding to RBD protein (left) or trimeric spike (right). The correlation for day 14 sera between neutralizing titer (log10) and ELISA binding titer (log10) was analyzed using Spearman nonparametric test. Line represents the best fit linear regression.
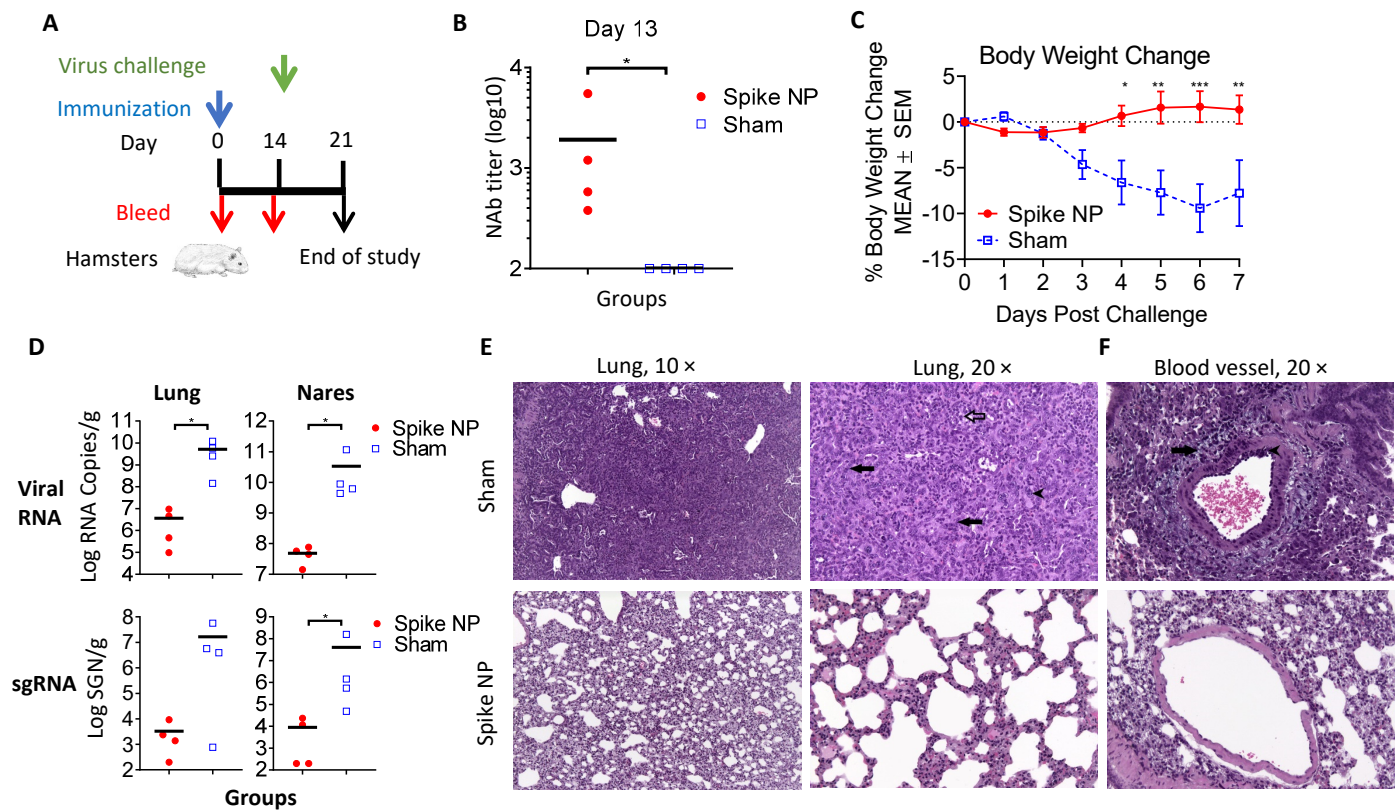
Figure 4. Vaccine protection efficacy against virus challenge in hamsters. (**A**) Schematic of the immunization and virus challenge protocol. Syrian golden hamsters (2F/2M) were immunized with 100 μg spike NP (REVC-128) or sham with Sigma Adjuvant System via intramuscular injection route, and challenged with 1.99×10^4 TCID$_{50}$ of SARS-CoV-2 virus (USA-WA1/2020, NR-53780, BEI Resources) by the intranasal route at day 14 post immunization. (**B**) The neutralizing activity of sera collected at day 13 post immunization against VSV pseudotyped virus containing SARS-CoV-2 spike with D614G mutation. Statistical analysis was performed with Mann-Whitney test (* $p < 0.05$). (**C**) Median percent weight change after challenge. Statistical analysis for body weight change was performed for comparison between spike NP and mock immunized animals by two-way ANOVA test, * $p < 0.05$, ** $p < 0.01$, *** $p < 0.001$. (**D**) Tissue viral loads on 7 dpi. Viral loads of lung (left) and nares (right) were measured by RT-PCR and quantitated as total viral RNA copies per gram tissue (upper) and subgenomic N RNA copies per gram tissue (bottom). Limitation of quantification is 200 copies/g. Black bars reflect mean responses. Statistical analysis was performed with Mann-Whitney test (* $p < 0.05$). SGN=Subgenomic N RNA copies. (**E, F**) Representative images of histopathology for lungs (**E**) and blood vessels (**F**) of sham control (upper) and spike NP (bottom) immunized animals. In a higher magnification of (**E**) on right (20 ×), black arrows indicate bronchiolo-alveolar hyperplasia characterized by hyperplastic epithelial cells extending from bronchioles and lining alveoli. Black arrowhead indicates hyperplastic cells with enlarged nuclei. Open arrow indicates mixed cell inflammation observed in alveolar lumen. In (**F**), black arrow indicates expansion of surrounding vascular tissue by edema (increased clear space and a pale basophilic material) and mononuclear cells. Black arrowhead indicates mononuclear inflammatory cells expanding the vessel wall (tunica media and intima).